Two vertical bars are located on the left side of the page: a wide, solid blue bar and a narrower, solid cyan bar to its right.

**NORSAR Scientific Report No. 2-2009**

# **Semiannual Technical Summary**

**1 January - 30 June 2009**

**Frode Ringdal (ed.)**

**Kjeller, August 2009**

## 6.2 Detection of aftershocks of the Feb 21, 2008 Spitsbergen M 5.9 event at ARCES

### 6.2.1 Introduction

An earthquake with magnitude 5.9 occurred on Feb, 21, 2008 (052:02.46.17.6) at Storfjorden-Heerland Svalbard region ( $77.01^{\circ}$  N,  $19.01^{\circ}$  E, depth 15.4 km, (Pirli *et al.*, 2009)). In the following few months, a great number of aftershocks kept happening. This area still showed increased seismicity a year later. Most aftershocks have magnitudes below 3. They are small regional events with regard to the ARCES array in Norway (Mykkeltveit *et al.*, 1987) at a distance of about 850 km. In this study, we apply the frequency-dependent Multi-Channel Wiener Filter (MCWF) to the ARCES array data.

The conventional array process method is delay-and-sum, also known as beamforming. This method maximizes the array response for the assumed direction and slowness of the coherent signal, but is not optimal because the coherent part of the seismic noise at each frequency usually will be concentrated at particular wavenumbers (Douglas, 1998). The MCWF optimizes the conventional beamforming by removing coherent noise from each trace before stacking. The principle of the MCWF is to use the noise on a number of reference traces to predict the noise on the primary channel, and then to subtract the predicted noise from the actual data. It is an adaptive process in which the frequency-dependent filters are determined by the data. It is thus suitable for use with passive seismic monitoring arrays in which the ambient noise might not be stationary. A complete procedure of the MCWF and the discussion about the algorithm can be found in Wang *et al.* (2009).

The ARCES array data is filtered by the MCWF. The SPITS array (Mykkeltveit *et al.*, 1992) at a distance of about 150 km provides reliable reference information on the true number of detectable aftershocks. This study aims to see how does the MCWF techniques help on the event detection by comparing with other methods, such as beamforming combined with band-pass filtering, the method employed by NORSAR.

When one attempts to detect small earthquakes from a large distance, the benefit of an array close to the source region is not always available. Therefore, an independent scheme is developed to apply the MCWF to the continuous data at ARCES during the period from Julian day 053 – 055, a period with a great number of aftershocks without too much overlap between events. The number of detected events from the MCWF filtered data are compared with that from the band-pass filtered data, both in the continuous mode.

### 6.2.2 Data Example

#### *Geometry*

NORSAR arrays: SPITS (at epicentral distance  $\sim 150$  km) and ARCES (at epicentral distance  $\sim 850$  km), and aftershocks from Storfjorden-Heerland Svalbard region are used for this study (see Fig. 6.2.1).

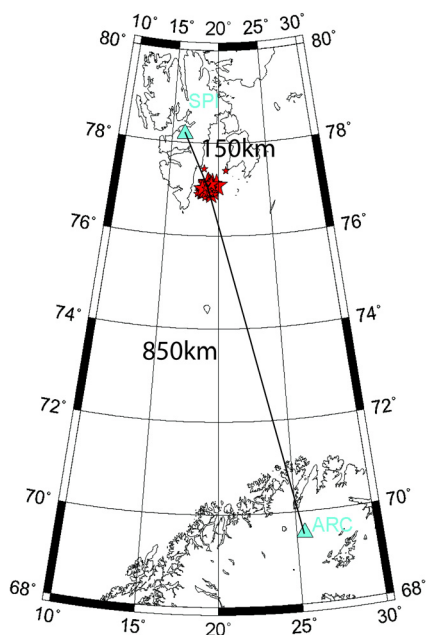


Fig. 6.2.1. Geometry of the source region (red stars) and the arrays SPITS and ARCES (blue triangles).

### Data

An aftershock with the origin time 2008.055:18.59.02 is used to demonstrate the improvement of the Signal-to-Noise-Ratio (SNR) by the application of MCWF. The Pg phase is detected by SPITS on 2008.055:18.59.26 with  $\text{SNR} = 290.8$  (calculated as ratio between the Short-Term and Long-Term Averaged amplitudes, STA/LTA). Based on the theoretical travel time difference between the source and arrays, SPITS and ARCES, the rough onset time of Pn arriving at ARCES is evaluated to be about 2008.055:19.00.58. Sixty seconds of ARCES array data (055:18:59:42 – 055:19:00:42), preceding the event, is taken as the noise reference data. The next 180 s during 055:19:00:42 – 055:19:03:42 is filtered by the MCWF. The window length of 5 s and the damping factor of 0.01 are used for the MCWF for the optimal results. Fig. 6.2.2 displays the band-pass filtered raw and individually filtered traces of the 25 vertical elements of the ARCES array. The band-pass filter always refers to a Butterworth filter at 3 – 8 Hz, with order 3, unless specifically indicated. Due to the weakness of the signals, it is difficult to tell the exact onset of the signals. But Pn and Sn are still visible and their arrival times match the expected aftershock signals for the ARCES array. The arrival of Pn and Sn are marked by arrows. By comparison, both events show stronger energy of the individually filtered traces than the band-passed raw traces. In fact, the NORSAR event detection program does not report this aftershock at the ARCES array as the NORSAR program uses an SNR threshold of 4.

### F-K analysis

The f-k analysis is an important tool for locating the direction from which the signal comes and its apparent velocity. However, weak signals would be easily misled by the high ambient noise in the f-k analysis. The Sn phase of the event at the origin time 2008.055:18.59.02 is used to demonstrate the improvement of the MCWF. Fig. 6.2.3 shows the enlarged Sn and the corresponding f-k analysis from the 25 vertical band-passed elements. Fig. 6.2.4 shows the enlarged Sn and the f-k analysis from 25 individually MCWF filtered traces. The f-k analysis of the individually MCWF filtered traces shows the expected signals, but the f-k analysis from the only band-passed data is smeared out by the noise.

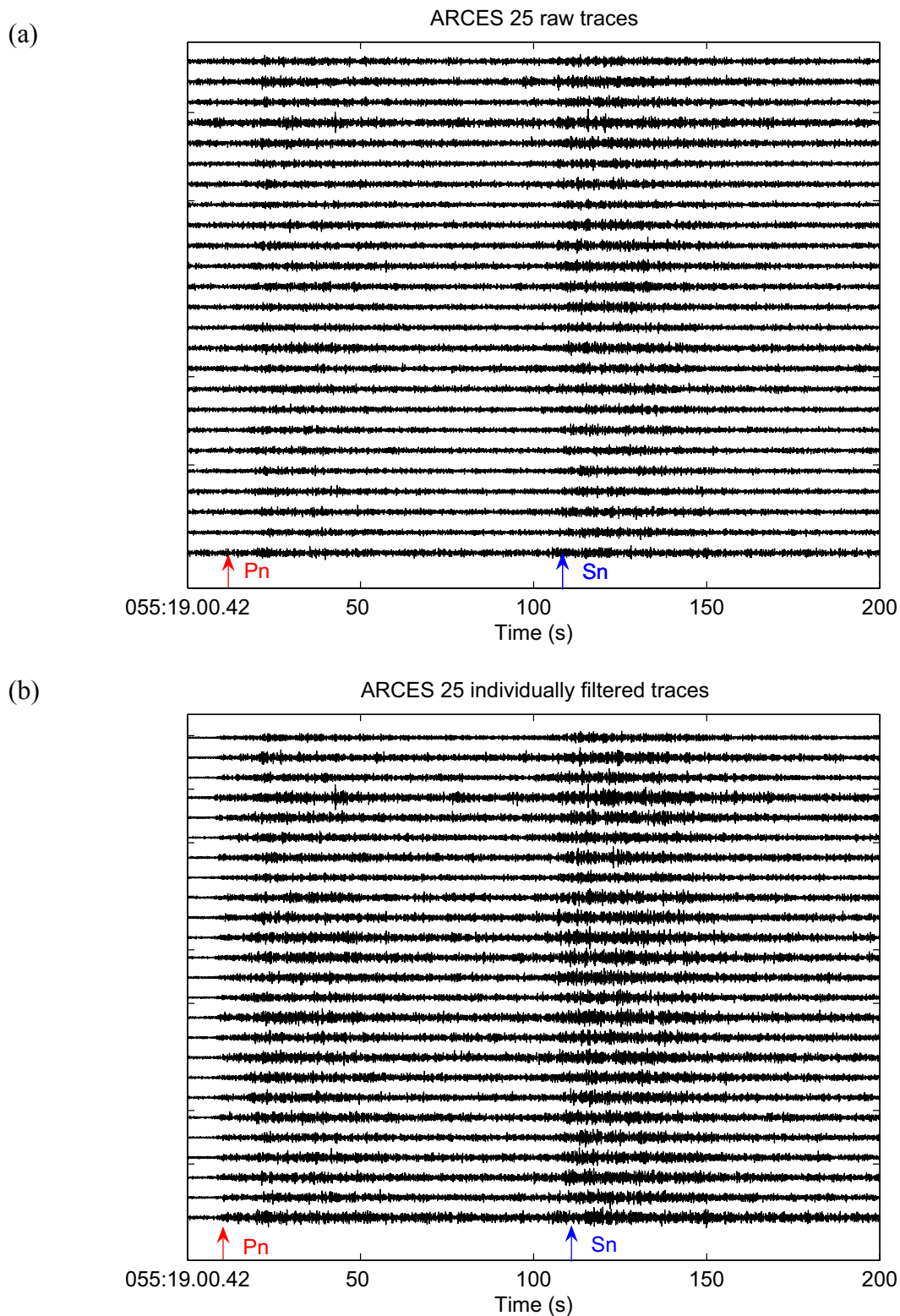


Fig. 6.2.2. Event with the origin time 2008.055:18.59.02. (a) Waveforms of the 25 vertical elements band-passed recordings at ARCES. (b) The band-passed waveform after individually MCWF filtered traces of the ARCES array. The arrival times are marked by red (Pn) and blue (Sn) arrows.

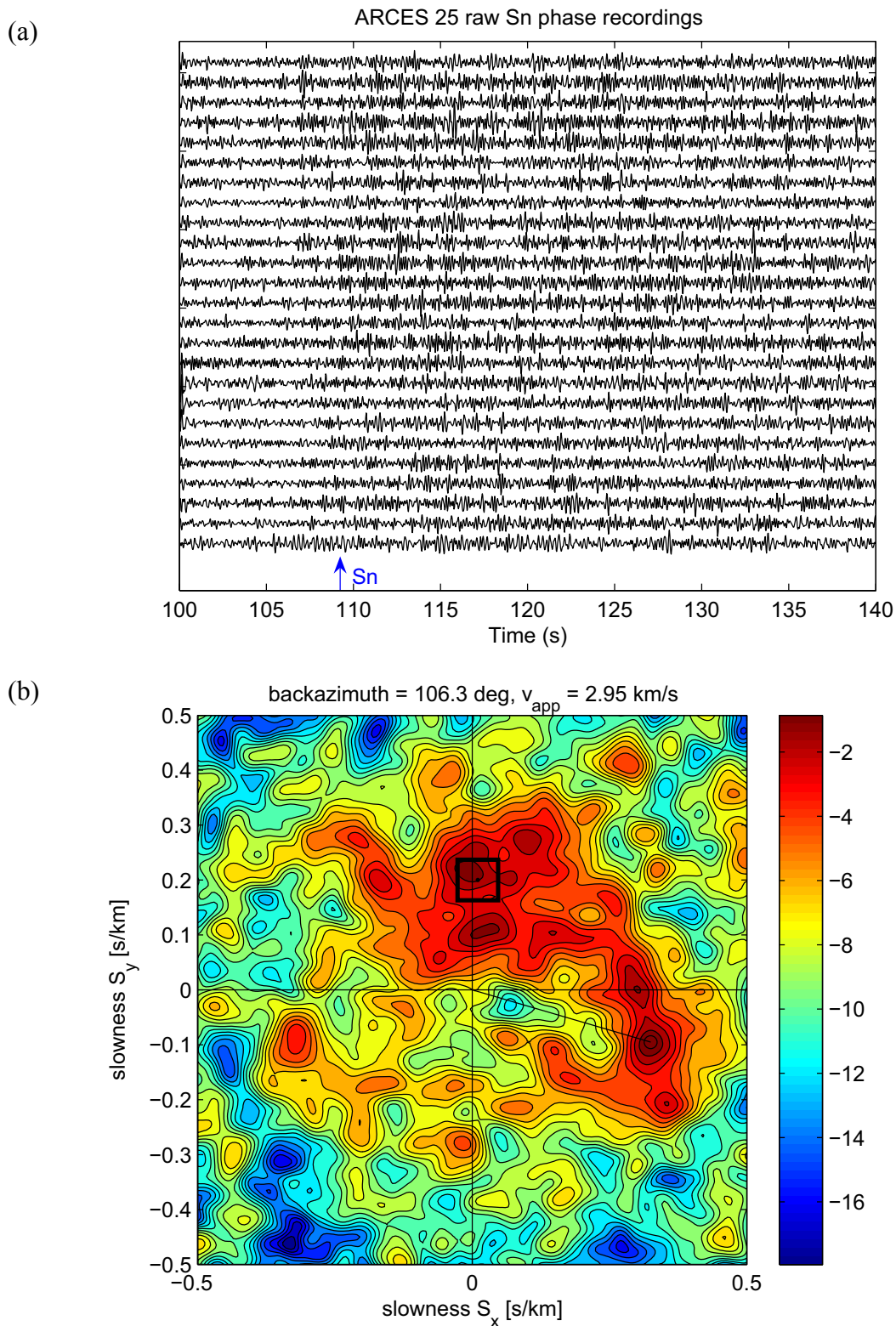


Fig. 6.2.3. Event with the origin time 2008.055:18.59.02. (a) Band-passed raw waveforms of Sn phases recorded by the ARCES array. The arrival is marked by the blue arrow. The start time is consistent with Fig. 6.2.2. (b) F-k analysis of individually filtered S waves over 109 – 111 s. The signal energy peak is expected in the black frame.

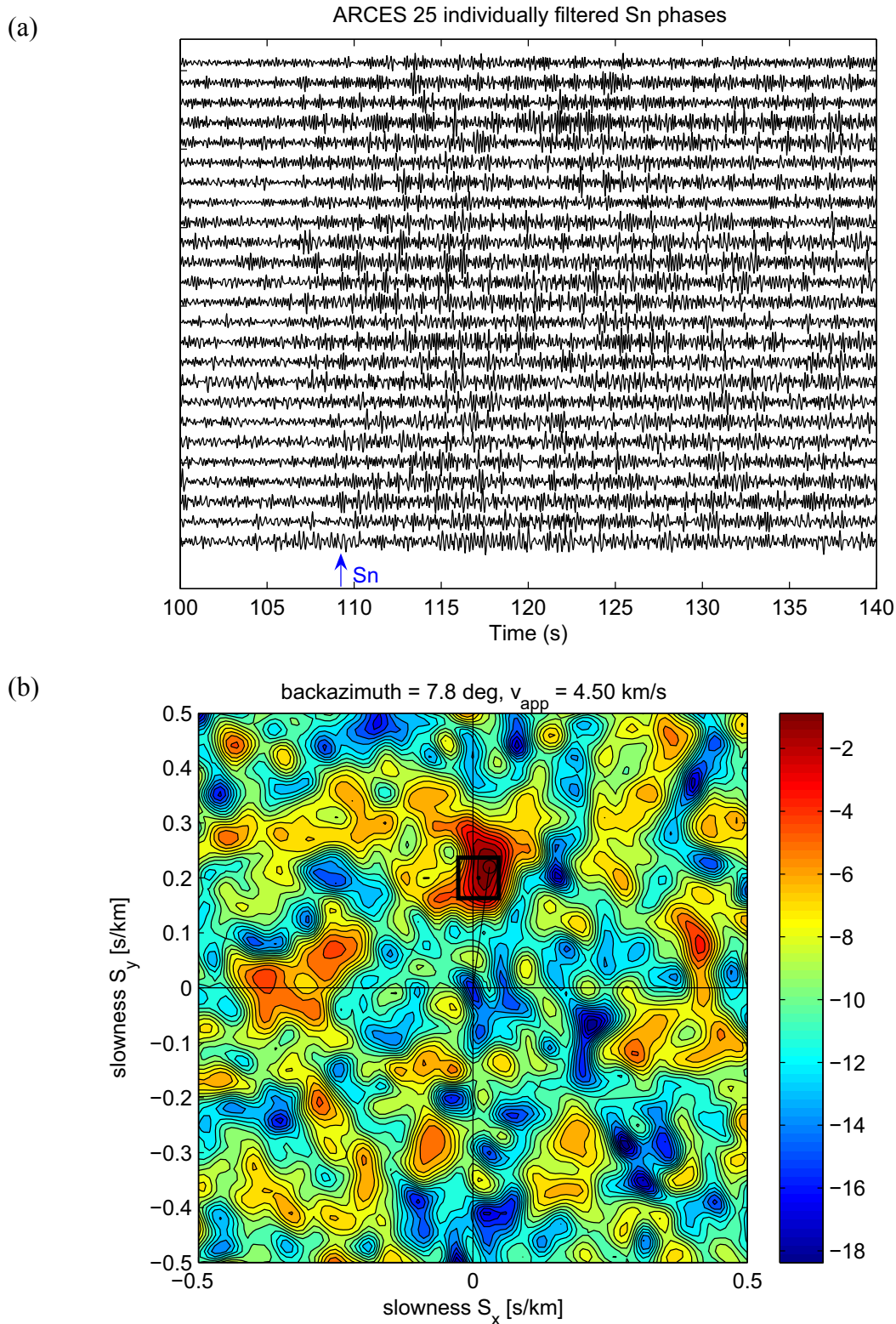


Fig. 6.2.4. Event with the origin time 2008.055:18.59.02. (a) Individually MCWF filtered waveforms combined with the band-pass filter, of Sn phases recorded by ARCES. The arrival is marked by the blue arrow. The start time is consistent with Fig. 6.2.2. (b) F-k analysis of individually filtered S waves over 109 – 111 s. The signal energy peak is expected in the black frame.

### 6.2.3 Event time indicated MCWF procedure

This section aims to detect aftershocks of the Spitsbergen main shock in the whole year of 2008. Detections by the SPITS array are used to define the possible windows in which aftershocks might be detected at ARCEN.

#### Work flow

As the SPITS array is much closer to the seismic source region than the ARCEN array, aftershocks with high SNR detected by ARCEN will also be detected by SPITS. On the other hand, the weaker aftershocks could be detected by the SPITS array, but might not necessarily be detected by the ARCEN array due to the much smaller signal amplitudes at ARCEN. Therefore, the detections by the closer SPITS array provide reliable reference time of aftershocks. The procedure of the MCWF application is summarized in four steps, some of them will be explained in detail later:

- Step I, select SPITS detections
- Step II, MCWF filters the ARCEN array data within the analysis time window defined by the SPITS detections and the Pn wave averaged travel time difference between ARCEN and SPITS
- Step III, do f-k analysis on each filtered candidate and select signals with the SNR above 3, and the back azimuth and apparent velocity falling into the expected range of the detected aftershocks reported by NORSAR's automatic regional bulletin (<http://www.norsardata.no/NDC/bulletins/gbf/2008.html>).
- Step IV, double check by eye

#### *Step I and Step II*

Fig. 6.2.5 shows the back azimuth and the apparent velocity of some aftershocks detected by both SPITS and ARCEN arrays as reported in the bulletin. These detections are made by the Generalized Beam Forming (GBF) method, the routine automatic NORSAR event location program (Ringdal & Kvernå, 1989). This plot gives the upper and lower limit of the detectable parameters of the potential aftershocks detected by both arrays. It is important to obtain these event parameters from the real observations rather than the theoretical calculation based on the location of the source and receiver, because of systematic slowness errors (Schweitzer, 2001). We use the back azimuth and apparent velocity range of 54 Pg phases detected by the SPITS array to set a search range of the SPITS detections for the whole year 2008. The back azimuth and apparent velocity of 46 Pn and Sn phase pairs detected by the ARCEN array are then used in step III to judge whether those declared candidates are aftershocks or not. The back azimuth searching range for Pg phase at SPITS is  $130 - 170^\circ$  and the apparent velocity range is  $4 - 8$  km/s according to Fig. 6.2.5. However, the initial searching ranges should be somewhat wider than that Fig. 6.2.5 suggests to ensure that no potential aftershocks are filtered out in the very beginning. This is because SPITS is much closer to the source region than ARCEN so that SPITS is more sensitive to the back azimuth of aftershocks than ARCEN. When more constraints are added in, the candidate events become clearer.

In total, there are 49857 detections claimed by the SPITS array during step I. The distribution of the SPITS detections with respect to the Julian day in 2008 is shown in Fig. 6.2.6. Among these detections, only those whose SNR at SPITS exceed 30 are assumed to be detectable by ARCEN.

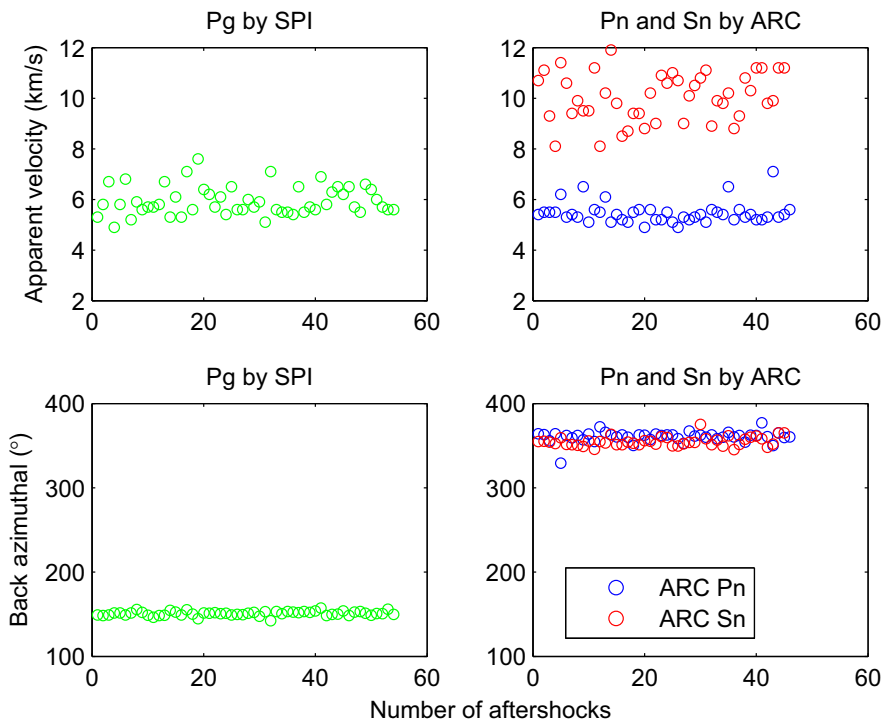


Fig. 6.2.5. Apparent velocity and back azimuth of the Pg phases (green) detected by the SPITS array and the Pn (red) and Sn (blue) phases detected by the ARCES array.

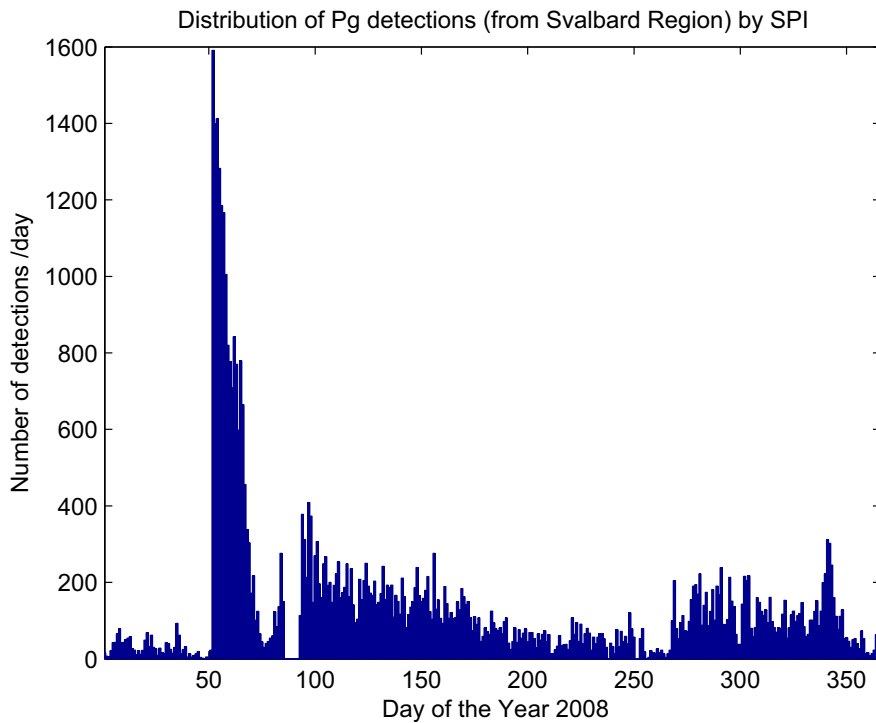


Fig. 6.2.6. Number of Pg detections by the SPITS array. The gap between Julian day 085 and 093 is due to an outage of the array.

5050 detections with SNR above 30 are found, about 10% of the total detections. An analysis time window for each detection is defined by the arrival time at SPITS and the average travel time difference to ARCES and SPITS. The ARCES array data in the analysis time window is filtered by the MCWF. A 60 s noise reference window is used to filter the next 180 s of data. A window length of 5 s and a damping factor of 0.01 are used.

The threshold of the SNR should not be so low that it includes a lot of noise, nor should it be so high as to reject many potentially detectable candidates. A SNR = 30 has proven to be a good threshold in this study. If the threshold of SNR is set to the lower value of 20, 2014 additional detections are made at SPITS, which will include many more candidates to be filtered (about 40%). A few of these additional events were checked and none of them were visible after the ARCES data is filtered by the MCWF.

Theoretically, the threshold of the SNR should not be the only parameter to select possible events candidates, because of the effect of the radiation pattern. If the SPITS array were to be near the nodal plane of a seismic event, the SNR will be much lower, but it could still be detected by the ARCES array. Therefore, using only the threshold of SNR runs the risk of missing some events. Fortunately, this case is not very likely and most of the potential candidates still fall into the selected range.

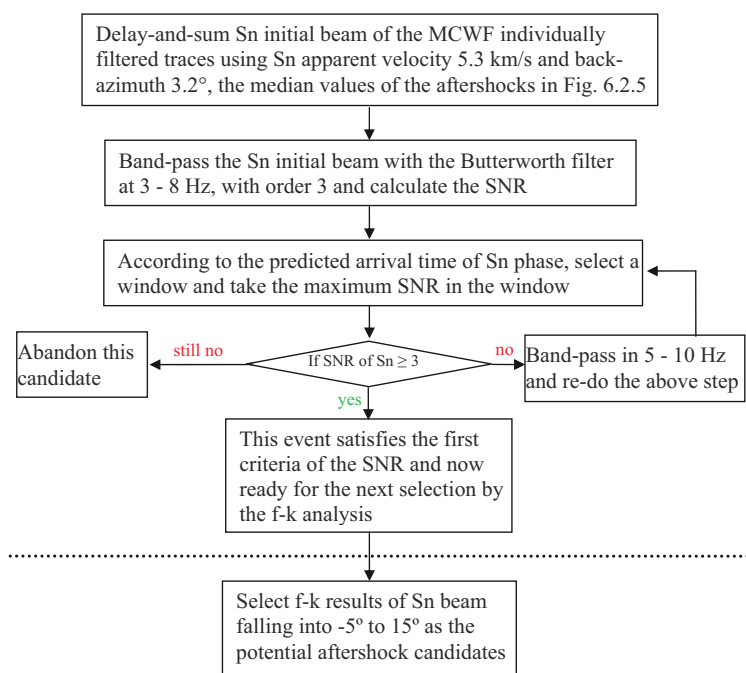


Fig. 6.2.7. The work flow for filtering and selecting aftershocks at ARCES. **Step III and Step IV**

Two criteria are used in this step to select potential aftershocks: (1) the SNR of the MCWF filtered Sn beam is above 3; (2) the f-k analysis results of back azimuth and apparent velocity that fall into the acceptable range. The detailed work flow is described in Fig. 6.2.7, where the two steps of selection are separated by a dashed line.

In this example, the SNR threshold, an empirical value, is based on the MCWF filtered Sn beam, rather than MCWF filtered Pn beam, because the energy of Sn is usually stronger than

Pn. There are quite a few cases where Pn is buried in the high ambient noise, but Sn still can be observed. In these cases, the SNR of Pn will be below the threshold and they are thus missed. The averaged back azimuth of  $355^\circ$  and apparent velocity of 10 km/s are used for delay-and-sum beamforming Pn and  $3.2^\circ$  and 5.3 km/s are used for delay-and-sum beamforming of Sn signals. The back azimuth difference between Pn and Sn is due to lateral heterogeneities along the travel path (Schweitzer, 2001).

After the candidates matching the first criterion are selected, the f-k analysis follows to further select the events. The choice of the appropriate window for f-k analysis is a tricky issue when the signal is weak. To overcome the uncertainty resulting from a single f-k analysis window, we ran a few windows around the predicted arrival time of the signals. For example, around the predicted arrival time of the Sn phase, we consider 20 s of individually MCWF filtered data. The f-k analysis is made in each moving 2 s window, with 50% overlap between neighbouring windows. For each f-k analysis, if the apparent velocity and back azimuth falls into the range of 3 – 7 km/s and  $-5$  to  $15^\circ$  the event is marked as a “true alarm”, otherwise as a “false alarm”. The search range of the apparent velocity and back azimuth is based on the statistical information of the well located aftershocks reported by the bulletin (see Fig. 6.2.5). The same procedure can also be applied to the Pn beam, except that the window length for f-k analysis is 1 s due to the higher frequency content of the Pn waves. Events with apparent velocity and back azimuth of f-k analysis of Pn falling into the 8 – 13 km/s and  $-10$  to  $10^\circ$  ranges, respectively, are marked as “true alarms”, otherwise as “false alarms”. The criterion of Pn will be used later in the automatic MCWF procedure. The more “true alarms” the candidate has, the more likely it is an aftershock event.

We found by inspection that the Sn beam on its own is a firm and stable constraint to judge whether a candidate detection is an event or not. The Sn beam should be used when the event is so weak that the f-k analysis of the Pn signal is scattered by the ambient noise and does not report the correct signal back azimuth and apparent velocity. It has also been found that the back azimuth is a more important factor than the apparent velocity as a criterion when the ambient noise degrades the f-k analysis. It means that when the back azimuth of the energy peak in the f-k analysis falls into  $-5$  to  $15^\circ$ , the apparent velocity would be within 3 – 7 km/s in most of cases. On the other hand, when the apparent velocity energy peak in the f-k analysis falls into the range 3 – 7 km/s, the back azimuth could be from all possible directions. Therefore, the actual criterion is set by the back azimuth only in the f-k analysis and it is shown to be a feasible and suitable criterion in practice. Finally, those Sn beams whose back azimuth fall into  $-5$  to  $15^\circ$  are accepted.

To summarize, among 5050 detections claimed by the SPITS array with an SNR above 30, there are 1085 detections with the SNR of Sn beam at ARCES above 3. 742 detections out of 1085 candidates are found whose Sn beam (from individual MCWF traces) satisfies the back azimuth criterion. By comparison, we repeat the same procedure of step III on the Sn beam of the band-passed raw data. Among 5050 detections at the SPITS array with the SNR above 30, we found 1021 detections with the SNR of Sn beam above 3. Only 694 detections out of 1021 candidates are found by the Sn beam (from band-passed raw data), based on the same back azimuth criterion. The candidates determined from the MCWF Sn beam and band-passed raw Sn beam are double-checked by eye in the last step. Both methods lose some candidate events off the thresholds in different stages. When the events are too weak, both methods will miss them.

Finally, 631 aftershocks are detected at ARCES in 2008. The Sn beam from the band-passed raw data detects 513 aftershocks with 181 false alarms. By comparison, the Sn beam from the individually MCWF filtered data found 577 aftershocks with 165 false alarms. The MCWF procedure found 10% more events and a 10% lower false alarm rate than the conventional beamforming combined with an appropriate band-pass filter.

These false event alarms occur due to several reasons. One of the main reasons is the disturbance by noise spikes. On some noisy days, a lot of spikes can be observed on the data. The MCWF cannot remove them because they are not predictable. Those spikes usually have high amplitudes, so that the first criterion (SNR larger or equal than 3) will be definitely satisfied. If the back azimuth of the f-k analysis happens to fall into the range  $-5$  to  $15^\circ$ , it will be accepted as a candidate. This problem can be partly solved by setting a proper apparent velocity criterion. However, a tight apparent velocity range runs the risk of rejecting some potential events when the signal is so weak that the apparent velocity reported by the f-k analysis has a large uncertainty. Another reason is that non-aftershocks from the same direction happen to occur at the same arrival time as aftershocks. This happened in a few cases but is easily excluded by eye. The third reason is due to the high level of ambient noise. In that case, the data usually shows nothing except for the stationary noise without spikes. The dominant ambient noise can come from the same direction as the signals so that it is mistaken as a real event by the f-k analysis.

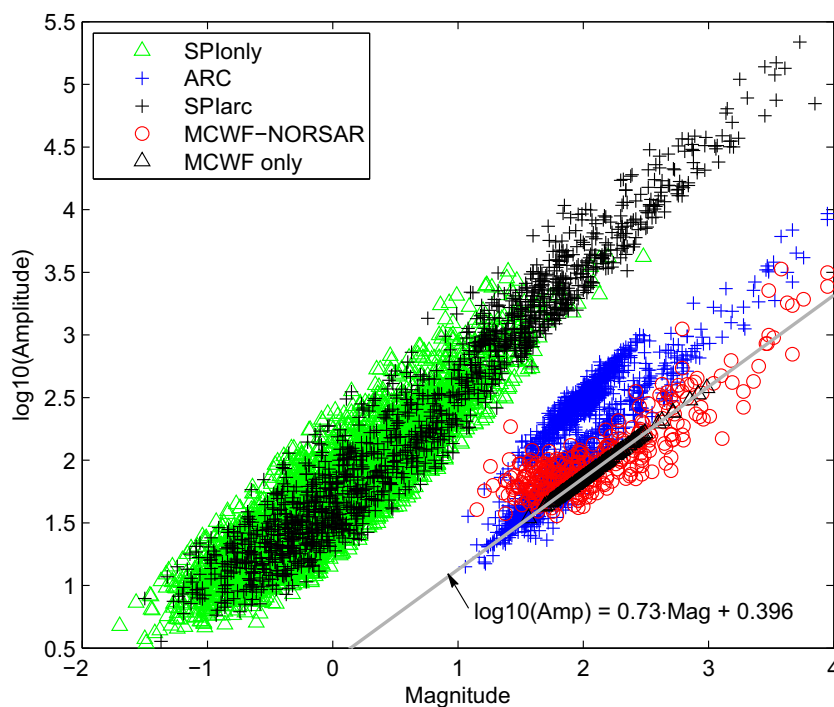


Fig. 6.2.8. The relationship between amplitude vs. magnitude of events. Black crosses are events detected by both SPITS and ARCES with amplitudes from the SPITS array data (NORSAR GBF processing). Green triangles are events detected by SPITS only. Blue crosses are events detected by both SPITS and ARCES with amplitudes from the ARCES array data (NORSAR GBF processing). Red circles are events detected at ARCES by both the MCWF procedure and the NORSAR GBF method with amplitude from the MCWF filtered results. The grey line is the least square line for the red circles, restricted to events with magnitudes larger than 2. Black triangles are events detected by the MCWF procedure only: as no reported magnitudes are available, they are plotted on top of the regression line.

### 6.2.4 Magnitude of aftershocks

The event identified MCWF procedure detected more events than the conventional beamforming method. Those events are missed by beamforming because of the low SNR. This section investigates the distribution of the magnitude of these missing events.

A list of events from the aftershock region is obtained from the NORSAR bulletins. The aftershock region is defined by longitude 17 to 21.3° E and latitude 76 to 77.6° N. The event location uses the GBF method. GBF automatically groups and locates seismic arrivals based on theoretical travel times for a grid of points covering a target area (Ringdal & Kværna, 1989).

The relationship between  $\log_{10}(\text{amplitude})$  and the reported magnitude of aftershocks is plotted in Fig. 6.2.8. The amplitude is the value of the beam with the best SNR. The magnitude is defined according to Båth *et al.* (1976).  $\log_{10}(\text{amplitude})$  and magnitude of both SPITS and ARCES detections follow a linear relationship.

Among 631 claimed aftershocks, there are 365 events reported by the GBF method. They are shown in Fig. 6.2.8 with red circles, with the amplitudes from the MCWF filtered results plotted against GBF defined magnitudes. As the MCWF differs from the GBF method, the amplitudes for the same events could be different. A regression line (see annotation in Fig. 6.2.8) is fit to those red circles (*i.e.*, MCWF amplitudes) with magnitudes larger than 2 because smaller events do not match the linear relationship well. The remaining events, which are detected by the MCWF procedure but not reported by the NORSAR bulletin, are plotted along the line with their  $\log_{10}(\text{amplitude})$  (black triangles in Fig. 6.2.8) based on the empirical relationship (grey line in Fig. 6.2.8) between  $\log_{10}(\text{amplitude})$  and magnitude.

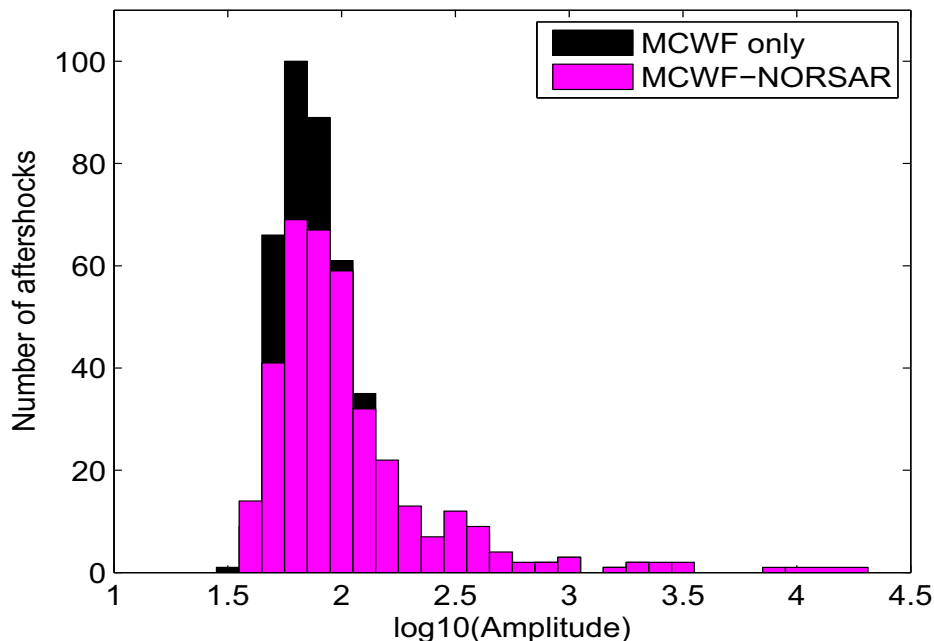


Fig. 6.2.9. Histogram of the number of detections against  $\log_{10}(\text{Amplitude})$ . The purple bars are events detected by both the MCWF procedure and NORSAR's GBF method. The black bars are events detected by the MCWF procedure only.

Fig. 6.2.9 shows the histogram of the number of event detections by both the NORSAR bulletin and the MCWF procedure (purple). The events detected by the MCWF procedure are plot-

ted in black, and those detected by the GBF method in purple. Therefore, it is clear that the MCWF procedure does not reduce much the magnitude of the smallest detectable event but instead detects additional aftershocks, mainly events whose  $\log_{10}(\text{amplitude})$  is between 1.7 and 2.

### 6.2.5 Automatic MCWF Procedure

In practice, event directions are not predictable in many cases. It would thus be required that the algorithm can filter events blindly, i.e., by filtering the continuous data with the MCWF without the benefit of prior information. As a test, the 3x24-hour continuous data on Julian days 053 – 055 are filtered continuously using the automatic MCWF detection procedure. Julian day 053 is one day after the main shock when there are not too many overlaps among aftershocks, but it still remains an active period.

The automatic MCWF procedure is to filter the whole data in a continuous mode and delay-and-sum to form the MCWF  $S_n$  beam. The  $S_n$  beam is used to select the events, instead of the  $P_n$  beam, because the  $P_n$  beam does not reliably detect weak aftershocks. The selection of aftershocks is conducted using the methods in Step III of section “Event Time Identified MCWF Procedure”, i.e., the SNR and the back azimuth of the  $S_n$  beam from the f-k analysis, are used to select the potential aftershocks. The five steps of the automatic MCWF procedure are (also see Fig. 6.2.10):

1. The first 120 s data is taken as the noise reference, which is used to filter the next 120 s of data. The filtered data are multiplied by a triangular window.
2. Take the data filtered in step 1 as the noise reference data for the next 120 s until the end of the continuous data.
3. Repeat these steps, but start the first window at 60 s instead.
4. Sum the results of steps 2 and 3 as individually filtered outputs.
5. The individually filtered outputs are delay-and-summed into the MCWF  $S_n$  beam by the back azimuth  $3.2^\circ$  and apparent velocity 5.3 km/s, the average value of aftershocks reported in Bulletin.

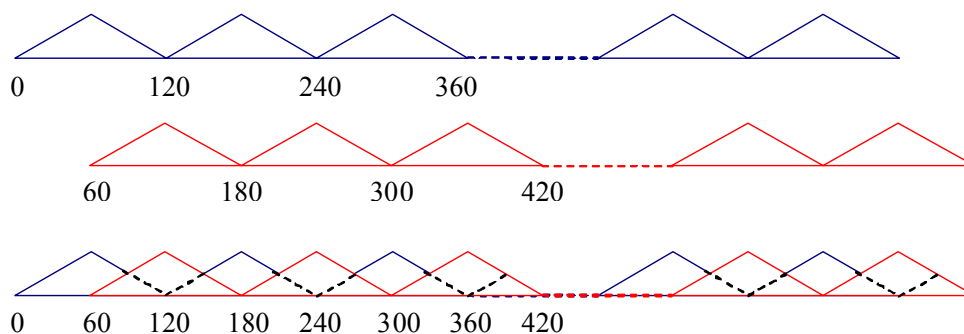


Fig. 6.2.10. The blue trace explains step 1 and 2 of the automatic MCWF procedure. In each window, the data is tapered by a triangular window. The red trace explains step 3, where the whole process is repeated but shifted half a window length. The sum of blue and red traces is the final result.

Theoretically, the SNR is supposed to be improved after being filtered. However, the window is updated by 50% overlap among windows in the automatic filtering process. It is thus possi-

ble that the automatic procedure does not use the proper noise reference data in some cases during filtering. For example, some events might happen to be split into two neighbouring windows, potentially including earthquake signals in the noise reference. This can be compensated in the next window with 50% overlap, but part of the signal is lost in the first round filtering step so that the SNR could be decreased a little. Therefore the SNR threshold to select the candidates should be set lower than 3, which is the value used in “Event Identified MCWF Procedure” Section, where the noise reference preceding the signal is properly chosen with the help of the reliable arrival time indication.

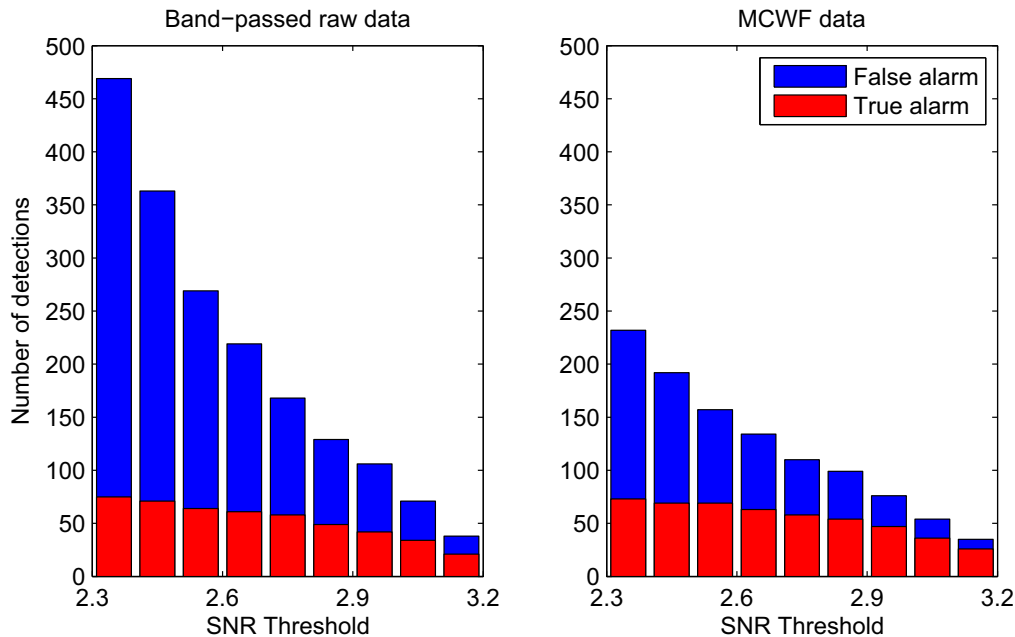


Fig. 6.2.11. The number of true and false detections as function of different STA/LTA thresholds. The number of false alarms is in blue. The number of true alarms is in red. The results detected by the band-passed raw data beamforming is shown in the left panel. The results from the automatic MCWF filtered data is shown in the right panel.

The appropriate threshold is investigated by trying a range between 2.3 and 3.2, with 0.1 increments. The number of detections by setting each threshold are demonstrated in Fig. 6.2.11. There are 78 events detected by band-passed raw data and 79 events detected by the MCWF filtered data when setting a SNR threshold of 2.3, both in automatic mode. The trade-off exists between detecting more events and including more false alarms. By comparison, the number of false alarms from band-passed raw data is significantly increased compared to the MCWF filtered data when the threshold is lower than 2.7. Therefore, a threshold of 2.7 is suggested to detect events as much as possible whilst keeping a moderate number of false alarms.

Fig. 6.2.12 demonstrates the improvement of the SNR of the automatic MCWF procedure. An event with the origin time 2008.054.08.35.51 is detected by the automatic MCWF filtered Sn beam, but missed by the delay-and-sum band-passed raw Sn beam. To keep the results comparable between the MCWF procedure and the NORSAR event detection program, we use the definition of SNR given by Schweitzer *et al.* (2002). A value of 6.0 is used for  $\zeta$ . The delay time  $\varepsilon = 5$  s for updating the LTA as compared to the STA. The STA window length is set to 1 s. The length of the short window is 0.25. A threshold (SNR = 2.7) is set in the SNR curves of both band-passed raw data and individually MCWF filtered results.

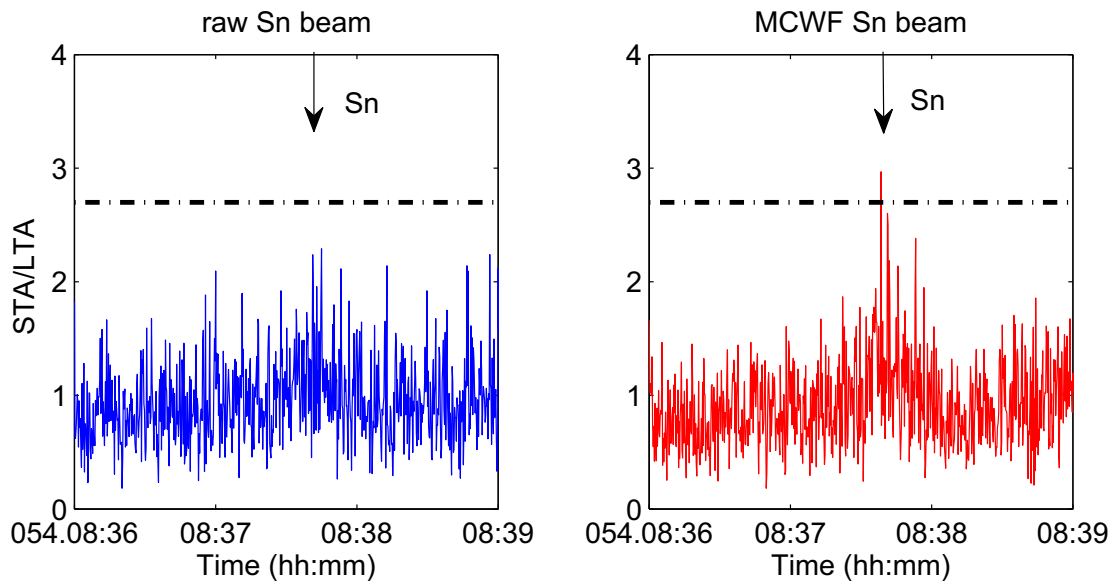


Fig. 6.2.12. Event with origin time 2008.054:08.35.51. Comparison of SNR curves of the band-passed raw Sn beam (blue) and the MCWF Sn beam (red) after the first stage automatic MCWF filtering. A threshold of SNR = 2.7 (black dashed line) in stage 1 is set for both cases. The expected Sn arrival is marked by an arrow.

### 6.2.6 Conclusion

The NORSAR arrays: SPITS and ARCES, and aftershocks from Storfjorden-Heerland Svalbard region are used to test the improvement of the MCWF on detecting weak regional events. The ARCES array data is filtered by the MCWF according to the time indicated by SPITS detections at a much closer distance than ARCES in 2008. Events are considered reliable when two criteria are satisfied: (1) a SNR threshold value is exceeded; (2) the back azimuth and apparent velocity determined from f-k analysis matches that of the average values of aftershocks. For comparison, instead of the MCWF filtered result, the band-passed raw ARCES array data indicated by the SPITS detection is band-passed and analyzed by the f-k method. The events from the band-passed raw data are judged by the same criteria. There are 631 aftershocks detected in the whole year of 2008. The conventional beamforming, detects 513 aftershocks with 181 false alarms; the multi-channel Wiener filtered results found 577 aftershocks with 165 false alarms. The MCWF procedure found 10% more events, whose  $\log_{10}(\text{amplitude})$  is between 1.7 and 2, and a 10% lower false alarm rate than the conventional beamforming combined with an appropriate band-pass filter.

The automatic MCWF procedure in the continuous mode found that the appropriate threshold of SNR for aftershock detection is 2.7. The MCWF also demonstrates the advantage of reducing the false alarms than the beamforming methods.

*Jingbo Wang, Bullard Laboratories, University of Cambridge*

*Johannes Schweitzer, NORSAR*

*Frederik Tilmann, Bullard Laboratories, University of Cambridge*

*Robert S. White, Bullard Laboratories, University of Cambridge*

## Acknowledgements

The research visit of Jingbo Wang at NORSAR was financed by the EC project NERIES (EC Contract Number 026130). University of Cambridge, Dept. Earth Sciences contribution No. ES1116.

## References

- Båth, M., O. Kulhanek, T. Eck & R. Wahlström (1976). Lateral inhomogeneities in the upper mantle. *Seismol. Inst., Uppsala, Tech. Report 5-76*, 37 pp.
- Douglas, A. (1998). Making the most of the recordings from short-period seismometer arrays. *Bull. Seism. Soc. Am.* **88**, 1155-1170.
- Mykkeltveit, S., F. Ringdal, J. Fyen & T. Kværna (1987). Initial results from analysis of data recorded at the new regional array in Finnmark, Norway. *NORSAR Sci. Rep.* **1-87/88**, 61-82.
- Mykkeltveit, S., A. Dahle, J. Fyen, T. Kvrerna, P.W. Larsen, R. Paulsen, F. Ringdal & I. Kuzmin (1992). Extensions of the Northern Europe Regional Array Network - New small-aperture arrays at Apatity, Russia, and on the Arctic island of Spitsbergen. *NORSAR Sci. Rep.* **1-92/93**, 58-71.
- Pirli, M., J. Schweitzer, L. Ottemöller, M. Raesi, R. Mjelde, K. Atakan, A. Guterch, S.J. Gibbons, B. Paulsen, W. Debski, P. Wiejacz & T. Kværna (2009). Preliminary Analysis of the 21 February 2008, Svalbard (Norway), Seismic Sequence. *Seism. Res. Lett.*, submitted.
- Ringdal, F. & T. Kværna (1989). A multi-channel processing approach to real time network detection, phase association, and threshold monitoring. *Bull. Seism. Soc. Am.* **79**, 1927-1940.
- Schweitzer, J. (2001). Slowness corrections - one way to improve IDC products. *Pure Appl. Geophys.* **158**, 375-396.
- Schweitzer, J., J. Fyen, S. Mykkeltveit & T. Kværna (2002). Seismic arrays. In: P. Bormann (ed.), *New manual of seismological observatory practice (NMSOP)*, Chap. 9, 52 pp.
- Wang, J., F. Tilmann, R.S. White & P. Bordonni (2009). Application of frequency-dependent multi-channel Wiener filters to event detection in 2D three-component seismometer arrays. *Geophysics*, in press.